Valence Characteristics and Structural Stabilities of the Electrolyte Solid Solutions $Ce_{1-x}RE_xO_{2-\delta}$ (RE = Eu, Tb) by High Temperature and High Pressure

Liping Li,[†] Guangshe Li,*[,‡] Yulu Che,[†] and Wenhui Su[†]

Department of Physics and Key Laboratory of Inorganic Synthesis and Preparative Chemistry, Jilin University, Changchun 130023, People's Republic of China, and International Centre for Materials Physics, Academia Sinica, Shenyang 110015, People's Republic of China

Received December 28, 1999. Revised Manuscript Received June 5, 2000

Solid solutions $Ce_{1-x}RE_xO_{2-\delta}$ (RE = Eu, Tb) were prepared by a high-temperature and -pressure method. The products were characterized by X-ray diffraction (XRD), TG, electron paramagnetic resonance (EPR), X-ray photoelectron spectroscopy (XPS), and Mössbauer spectroscopy. XRD data analysis showed that all solid solutions crystallized in a single-phase cubic fluorite structure. The nonlinear relationships between the lattice parameter and dopant content for both series of solutions were ascribed to the results of cation substitutions and variations of the relative content of oxygen vacancy Vö and defect associations $\{RE'_{Ce}Vö\}$ and $\{Ce'_{Ce}Vö\}$. EPR and XPS measurements confirmed the presence of Ce^{3+} ions in the solid solutions. For the solid solutions $Ce_{1-x}Eu_xO_{2-\delta}$, all Eu ions were determined to be trivalent by XPS and ^{151}Eu Mössbauer measurements. For the solutions $Ce_{1-x}Tb_xO_{2-\delta}$, all Tb ions were also stabilized in the trivalent state. This result is different from that of the counterpart by hydrothermal conditions, in which a mixed valence of Tb^{3+}/Tb^{4+} prevails at a higher dopant content. The prepared solutions $Ce_{1-x}Tb_xO_{2-\delta}$ were metastable. With increasing temperature, they would be destabilized and decompose into two fluorite phases, accompanied by partial oxidation from Tb^{3+} to Tb^{4+}. Alternating current impedance spectroscopy showed primarily bulk conduction for all samples. For the solutions $Ce_{1-x}Eu_xO_{2-\delta}$, the temperature dependence of the ionic conductivity was linear within the temperature range measured with activation energies of 1.05, 0.82, and 0.87 for $x = 0.2$, 0.38, and 0.5, respectively. For the decomposition product of the solid solution $Ce_{0.71}Tb_{0.29}O_{2-\delta}$, the conductivity gave two linear regions with smaller activation energies; i.e., the activation energy was 0.60 eV below 600 °C and 0.39 eV above 600 °C. The higher ionic conductivity (1.1×10^{-2} S/cm at 720 °C) for the decomposition phases of the solution $Ce_{0.71}Tb_{0.29}O_{2-\delta}$ was ascribed to an electronic component involved in relation to the presence of the mixed valence of Tb^{3+}/Tb^{4+} and Ce^{3+}/Ce^{4+}.

Solid electrolytes with high oxide ion conductivities have been attracting great interest for application in high-temperature fuel cells and oxygen sensors. The electrolytes widely investigated are fluorite-type oxides.[1,2] The ZrO_2-based electrolytes, e.g., yttria-stabilized zirconia (YSZ), exhibit very good mechanical properties and relatively high oxide ion conductivity. Bi_2O_3-based solid solutions have been considered as the alternative electrolytes with very high oxide ion conductivities at moderate temperature; however, the electronic component cannot be negligible in some cases.

Another promising high-conducting solid electrolyte is doped ceria, which has a relatively high thermal stability. A large amount of intrinsic and extrinsic oxygen vacancies existing in the doped ceria provide the passages for oxide ion hopping. The intrinsic vacancies arise from the presence of Ce^{3+} ions in the fluorite lattice due to the reduction equilibrium of Ce^{3+}/Ce^{4+}, whereas the extrinsic oxygen vacancies and further oxygen concentrations in these solid solutions are controlled by substitutions of aliovalent ions for cerium in the lattice. The preparation and transport properties of the solid electrolytes CeO_2 doped with rare earth and/or other aliovalent ions have been investigated by many researchers.[3−5] Greenblatt et al. have systematically synthesized solid solutions $Ce_{1-x}Sm_xO_{2-x/2}$ and $Ce_{1-x}Ca_xO_{2-x}$ by hydrothermal conditions.[3] They found that the ionic conductivity increased with increasing Sm (Ca) substitution, reached a maximum at $x = 0.17$ (0.09), and then decreased. The presence of a conductivity

* Corresponding address: Research Center of Supercritical Fluid Technology, Chemical Engineering Department, Tohoku University, Sendai 980-8579, Japan. E-mail: guangshe@scf.che.tohoku.ac.jp or Lp_Li@hotmail.com.
† Department of Physics, Jilin University.
‡ Key Laboratory of Inorganic Synthesis and Preparative Chemistry, Jilin University.

(1) Boivin, J. C.; Mairesse, G. *Chem. Mater.* **1998**, *10*, 2870.
(2) Huang, K.; Feng, M.; Goodenough, J. B. *Solid State Ionics* **1996**, *89*, 17.
(3) Huang, W.; Shuk, P.; Greenblatt, M. *Chem. Mater.* **1997**, *9*, 2240.
(4) Li, G.; Mao, Y.; Li, L.; Feng, S.; Wang, M.; Yao, X. *Chem. Mater.* **1999**, *11*, 1259 and references therein.
(5) Shuk, P.; Greenblatt, M.; Croft, M. *Chem. Mater.* **1999**, *11*, 473.

10.1021/cm990803p CCC: $19.00
Published on Web 08/31/2000

maximum and activation energy minimum with dopant content had been ascribed to the formation of the defect associations of the types $\{Sm'_{Ce}V\ddot{o}\}$ and $\{Ca''_{Ce}V\ddot{o}\}$ for Sm and Ca substitution systems, respectively. For the solid solutions $(CeO_2)_{1-x}(BiO_{1.5})_x$, however,[4] the solution limit was as high as $x = 0.50$, and the ionic conductivity and activation energy showed opposite changes with dopant content to those of the solid solutions $Ce_{1-x}Sm_xO_{2-x/2}$ and $Ce_{1-x}Ca_xO_{2-x}$.[3] It is reasonable that the chemical nature and valence states of the dopant ions determine the structural and physical properties of the ceria-based electrolytes.

Rare earth ions, e.g., Ce, Pr, Eu, and Tb, have special chemistry features, that is, their variable valence characteristics. The ionic valences are significantly influenced by the chemical natures of the host ions as well as the synthetic routes. For example, the metal oxide materials containing Eu^{2+} can be obtained by atmosphere reduction of Eu^{3+} ions on the basis of the standard reduction potential of -0.36 eV.[6] Recently, we used $Eu_2{}^{3+}O_3$ as the starting material and successfully prepared some perovskite oxides with a mixed valence of Eu^{3+}/Eu^{2+} by high-temperature and -pressure synthesis.[7] We have shown that Tb^{3+} ions could be stabilized by high-temperature and -pressure synthesis,[8] although the starting material used was a metal oxide containing Tb^{4+}. Because the valence states of the dopant ions in the CeO_2-based oxide electrolytes often play the predominant role in controlling the structural stability and transport property of the final products, it is of great importance to stabilize specific valences of the dopant ions in the fluorite lattice, especially when the dopant ions are rare earth metals of variable valences.

In this paper, we report on the stabilization of Eu^{3+} and Tb^{3+} ions in the fluorite lattice by high-pressure and -temperature synthesis of the solid solutions $Ce_{1-x}RE_xO_{2-\delta}$ (RE = Eu, Tb). The valence characteristics, structural stabilities, and transport properties for these solid solutions are determined and discussed.

Experimental Section

Chemicals Eu_2O_3 (A.R.), Tb_4O_7 (A.R.), and CeO_2(A.R.) were used as the starting materials. They were weighed according to the ratios of $Ce_{1-x}RE_xO_{2-\delta}$ ($x = 0.00$, 0.10, 0.17, 0.20, 0.29, 0.38, 0.44, 0.50 for RE = Eu, and $x = 0.00$, 0.10, 0.17, 0.29, 0.38 for RE = Tb). After the chemicals were thoroughly mixed, the mixtures were preheated at 900 °C for 5 h at ambient pressure to remove completely the carbonate species absorbed on the sample surface and to initiate partial reactions. The preheated samples were detected by powder XRD to be the mixtures of the starting component oxides. These mixtures were put into a high-pressure chamber as illustrated in the literature.[7] A belt-type apparatus was used to synthesize the samples. The pressure was loaded to 3.6 GPa. The temperature was then increased gradually to 1000 and 900 °C for the samples containing Eu and Tb, respectively. After being kept at high pressure and high temperature for 30 min, the specimens were quenched to room temperature under high pressure. Finally, the pressure was released and the pellet samples were obtained.

Powder X-ray diffraction data for the samples were collected at room temperature on a Rigaku 12-kW copper rotating anode X-ray diffractometer. The scan rate is 0.3° 2θ/min. Silica powder (99.99% pure) was used as the internal standard for peak position determination. The lattice parameters for the solid solutions were determined by least-squares methods. Thermogravimetric (TG) curves for the samples were recorded on a PE-DTA 1700-TGA7 PC thermoanalyzer in air at a heating rate of 10 °C/min.

The valence states of the Ce, Eu, and Tb ions for the solid solutions were determined by X-ray photoelectron spectroscopy (XPS). The XPS spectra for powder samples fixed on double-sided tapes were measured on an ESCA-LAB MK II X-ray photoelectron spectrometer from VG Co. with Al Kα radiation; the base pressure was 10^{-7} Pa. The C_{1s} signal was used to correct the charge effects on the sample surface.

The electron paramagnetic resonance (EPR) measurements were carried out at 80 K on a BRUKER ER200D spectrometer. A frequency of ca. 9.77 GHz was used for a dual-purpose cavity operation. The magnetic field of ca. 0.32 mT was modulated at 100 kHz. A microwave power of ca. 6.5 mW was used. Reference signals of Mn^{2+} in MgO crystals were used as the standard for the precise effective *g*-factor value.

^{151}Eu Mössbauer spectra of the samples $Ce_{1-x}Eu_xO_{2-\delta}$ were recorded at room temperature on an OXFORD MS-500 constant acceleration spectrometer. The velocity was calibrated with an α-Fe foil. The radiation source was $^{151}Eu/SmF_3$. The thickness of the absorber used in the measurements was ca. 6−15 Eu mg/cm^2. The experimental Mössbauer data were fitted by superimposing Lorentzians.

The opposite sides of the pellet samples were coated with silver paste and heated to 550 °C in air for half an hour so as to remove completely the organic components in the paste. The ionic conductivities for the pellet samples were measured using a Solatron 1260 impedance/gain-phase analyzer with an alternating current having a frequency between 5 Hz and 13 MHz at an amplitude of 50 mV in the temperature range of 350−750 °C in air.

Results and Discussion

1. Structural Characteristics of the Solid Solutions $Ce_{1-x}RE_xO_{2-\delta}$ (RE = Eu, Tb) by High-Temperature and -Pressure Synthesis. During the high-temperature and -pressure synthesis, the temperature and pressure are two main parameters influencing the crystallization of single-phase products. For the present work, we find that the synthesis temperature is crucial for the formation of single-phase solutions $Ce_{1-x}RE_xO_{2-\delta}$ (RE = Eu, Tb). When the pressure loaded is fixed as 3.6 GPa, reactions at a temperature below 800 °C usually give mixtures containing unreacted component oxides, e.g., Eu_2O_3, Tb_4O_7, and CeO_2. The optimum preparative temperature is 1000 °C for $Ce_{1-x}Eu_xO_{2-\delta}$ and 900 °C for $Ce_{1-x}Tb_xO_{2-\delta}$, respectively. It should be mentioned that the formation temperatures for these solutions are usually above 1400 °C at ambient pressure by traditional solid-state reactions.

The powder XRD patterns are measured for the solutions $Ce_{1-x}RE_xO_{2-\delta}$ (RE = Eu, Tb) prepared by a high-temperature and -pressure method. All diffraction peaks for $Ce_{1-x}Eu_xO_{2-\delta}$ (Figure 1) and $Ce_{1-x}Tb_xO_{2-\delta}$ (Figure 2) are highly symmetric and match well with the diffraction data for the standard fluorite structure. No XRD patterns for the component oxides, e.g., Eu_2O_3, Tb_4O_7, and CeO_2, are detected. Therefore, the XRD data for these samples in Figures 1 and 2 can be indexed in a cubic symmetry.

The relationships between the lattice parameter and substitution content of Eu (Tb) ions (x) are shown in

(6) Lide, D. R., Ed. *CRC Handbook of Chemistry and Physics*, 74th ed.; CRC Press: Boca Raton, FL, 1989.
(7) Lu, D.; Li, L.; Miao, J.; Liu, H.; Su, W. *Rev. High-Pressure Sci. Technol.* **1998**, *7*, 1031.
(8) Li, L.; Wei, Q.; Liu, H.; Su, W. *Z. Phys. B* **1995**, *96*, 451.

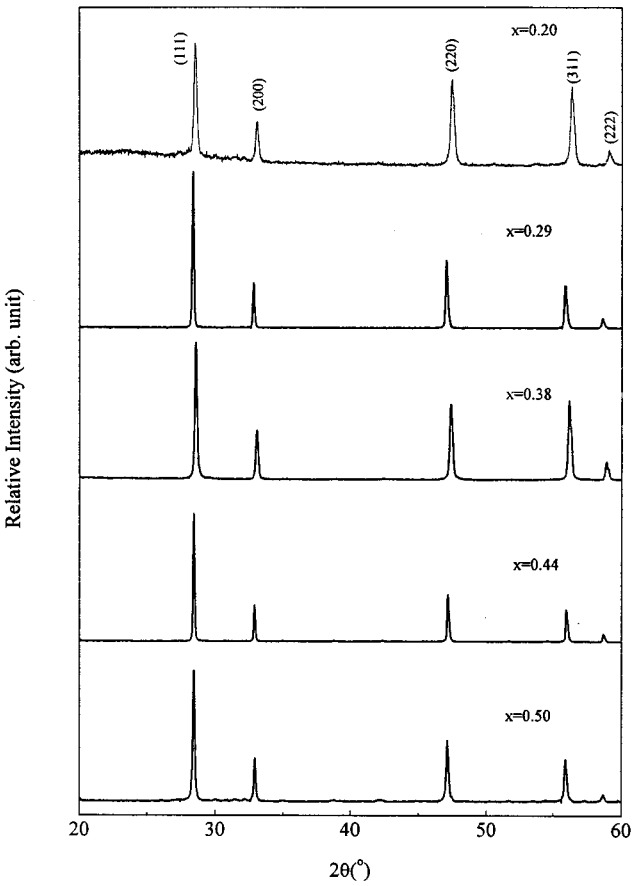

Figure 1. XRD patterns for the typical solid solutions $Ce_{1-x}Eu_xO_{2-\delta}$ (x = 0.20, 0.29, 0.38, 0.44, 0.50) by high-temperature and -pressure synthesis.

Figure 3. The lattice parameter for the undoped ceria treated by high-temperature and -pressure is 0.5410(1) nm, in good agreement with that reported for pure ceria (JCPDS, 34-394). With increasing dopant content x, the lattice parameter for the solid solutions $Ce_{1-x}Eu_xO_{2-\delta}$ increases (Figure 3a). When the dopant content is higher than $x = 0.4$, the lattice parameter for the fluorite phase keeps near the same. This trend seems to coincide with the effective ionic radius of Eu^{3+} ions (0.1206 nm) larger than that of Ce^{4+} (0.111 nm) with 8-fold coordination;[9] however, as shown in Figure 3a, the relationship between the lattice parameter and substitution content is nonlinear. To explain this nonlinear relationship, two points should be emphasized here: (i) all Eu ions are present as Eu^{3+} in our solid solutions, as determined by the following XPS and Mössbauer measurements and (ii) a mixed valence of Ce^{3+}/Ce^{4+} exists in the solid solutions, as confirmed by the following EPR and XPS. The increasing trend for the lattice parameter with dopant content is essential because of the larger ionic radius of dopant Eu^{3+}. However, as known in the ceria-based solid solutions,[4] every two Eu^{3+} dopants or Ce^{3+} ions from the reduction equilibrium, Ce^{4+}/Ce^{3+}, will generate one oxygen vacancy Vö in the fluorite lattice of the solid solutions $Ce_{1-x}Eu_xO_{2-\delta}$; the influence of the oxygen vacancy on the lattice parameter is contrary to that resulting from the cation substitution. On the other hand, in the doped fluorite

(9) Shannon, R. D. *Acta Crystallogr.* **1976**, *A32*, 751.

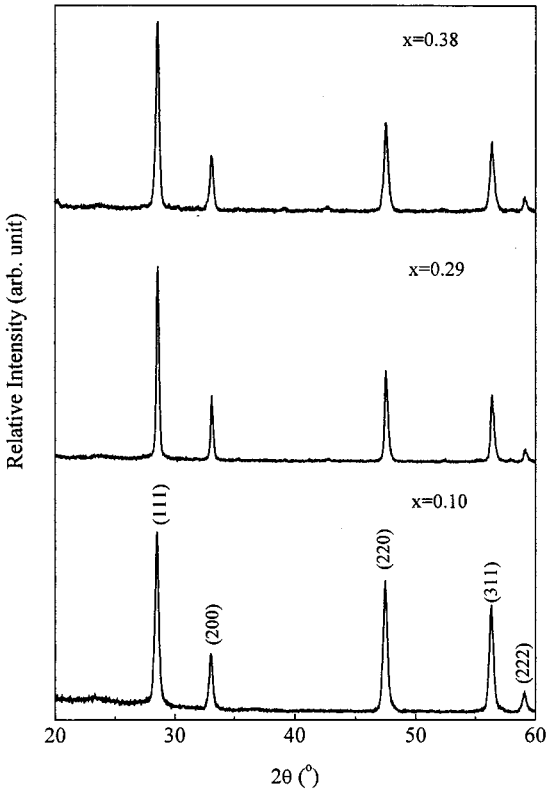

Figure 2. XRD patterns for the typical solid solutions $Ce_{1-x}Tb_xO_{2-\delta}$ (x = 0.10, 0.29, 0.38) by high-temperature and -pressure synthesis.

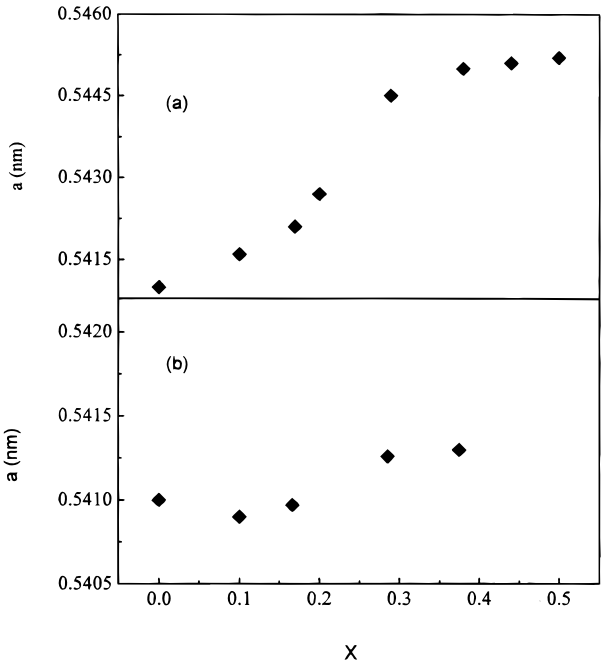

Figure 3. Relationship between the lattice parameter and dopant content (x) for the solid solutions $Ce_{1-x}Eu_xO_{2-\delta}$ (a) and $Ce_{1-x}Tb_xO_{2-\delta}$ (b).

lattice, there exist some changes of the relative contents of the oxygen vacancy Vö and the localized defect associations[3,4] (e.g., $\{Eu'_{Ce}Vö\}$ and $\{Ce'_{Ce}Vö\}$ for the present solutions $Ce_{1-x}Eu_xO_{2-\delta}$) with the increasing dopant content; i.e., the number of oxygen vacancies Vö in the solutions will first increase with dopant content and reach a maximum at a certain dopant

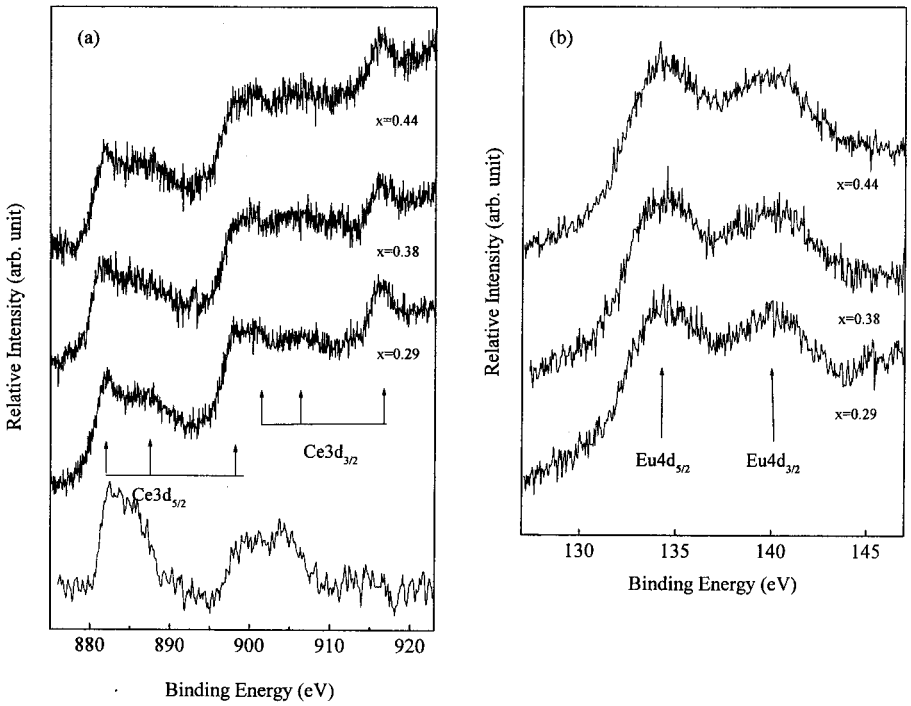

Figure 4. Core level XPS of Ce_{3d} (a) and Eu_{4d} (b) for the solid solutions $Ce_{1-x}Eu_xO_{2-\delta}$ ($x = 0.29, 0.38, 0.44$). A typical differential spectrum of Ce_{3d} signal is shown at the bottom of Figure 4a using the standard CeO_2 by hydrothermal conditions as reference;[10] the two distinct peaks at ca. 884.0 and 900.0 eV clearly indicate the presence of some Ce^{3+} ions in present solid solutions.

content x, and then the defect associations begin to form.[3] Oxygen vacancy Vö and defect associations $\{Eu'_{Ce}Vö\}$ and $\{Ce'_{Ce}Vö\}$ appearing in the present solutions are surely to have different interactions with the network ions, and the oxygen vacancy Vö is believed to produce a larger lattice contraction than the defect associations. The nonlinear relationship between the cell parameter and dopant content is a consequence of cation substitution and variations of the relative contents of oxygen vacancy Vö and these defect associations.

The relationship between the lattice parameter and dopant content x for the solid solutions $Ce_{1-x}Tb_xO_{2-\delta}$ (Figure 3b) is a little more complex than that for the solutions $Ce_{1-x}Eu_xO_{2-\delta}$ (Figure 3a). The lattice parameter first decreases slightly ($x < 0.1$) and then increases readily ($x > 0.1$) with the dopant content x. Here, we should recall the relative ionic radii of Tb^{3+} and Tb^{4+} to Ce^{4+}.[9] The ionic radius for Tb^{3+} is 0.118 nm, slightly larger than that of Ce^{4+} (0.111 nm), while that of Tb^{4+} (0.102 nm) is smaller than that of Ce^{4+}. Accordingly, Tb^{3+} substitution in the fluorite lattice of the solutions $Ce_{1-x}Tb_xO_{2-\delta}$ will be followed by an expansion of the lattice, while Tb^{4+} substitution will lead to a contraction of the fluorite lattice. Greenblatt et al.[5] reported a decrease of the lattice parameter with the Tb content in $Ce_{1-x}Tb_xO_{2-\delta}$, which was closely related to the existence of Tb^{4+} ions. For our solid solutions $Ce_{1-x}Tb_xO_{2-\delta}$, the relationship between lattice parameter and dopant content is expected to be drastically different from the solid solutions $Ce_{1-x}Eu_xO_{2-\delta}$ and the hydrothermally synthesized $Ce_{1-x}Tb_xO_{2-\delta}$ because (a) only Tb^{3+} ions were present in our solid solutions, as confirmed by the following XPS measurements, and (b) the dopant Tb^{3+} in $Ce_{1-x}Tb_xO_{2-\delta}$ has an ionic radius much closer to Ce^{4+}, whereas in the solutions $Ce_{1-x}Eu_xO_{2-\delta}$ there exists a larger ionic size difference between Eu^{3+} and Ce^{4+}. Therefore, at a lower dopant content x, Tb^{3+} substitution has a smaller influence on the lattice parameter variation in comparison with the oxygen vacancy involved, while its influence will be larger with increasing dopant content. On the basis of such a consideration, we ascribe the slight decrease of the lattice parameter with dopant content $x < 0.1$ in Figure 3b to the presence of a large amount of oxygen vacancies, while the gradual increase of the lattice parameter at higher dopant content to the Tb^{3+} substitution along with the formation of defect associations of $\{Tb'_{Ce}Vö\}$ and $\{Ce'_{Ce}Vö\}$.

2. Valence Characteristics for the Solid Solutions $Ce_{1-x}RE_xO_{2-\delta}$ (RE = Eu, Tb). To investigate the valence states of Ce, Eu, and Tb ions in the solid solutions $Ce_{1-x}RE_xO_{2-\delta}$ (RE = Eu, Tb), XPS spectra were measured at room temperature. The core level spectra of Ce_{3d} and Eu_{4d} for the solid solutions $Ce_{1-x}Eu_xO_{2-\delta}$ are illustrated in Figure 4. The $Ce_{3d_{5/2}}$ signals for the solid solutions clearly consist of three photoelectron peaks, which are in a binding energy sequence assigned to the $4f^0$, $4f^1$, and $4f^2$ final configuration states arising from the strongly mixed states between the $4f^0$ and $4f^1$ initial configuration state for Ce^{4+}. A similar spectrum had been obtained for our solid solutions $(CeO_2)_{1-x}(BiO_{1.5})_x$.[4] It is worth noting that this result is slightly different from CeO_2;[10] especially the resolution of Ce_{3d} spectra for the present solid solutions containing Eu is poor and the peaks corresponding to these three final states are not well defined. Romeo et al.[11] studied the reduction of ceria by XPS. They proposed that the photoemission peak at ca. 916.0 eV

(10) Li, G.; Feng, S.; Li, L. *J. Solid State Chem.* **1996**, *126*, 74.
(11) Romeo, M.; Kak, K.; El Fallah, J.; Le Normand, F.; Hilaire, L. *Surf. Interface Anal.* **1993**, *39*, 508.

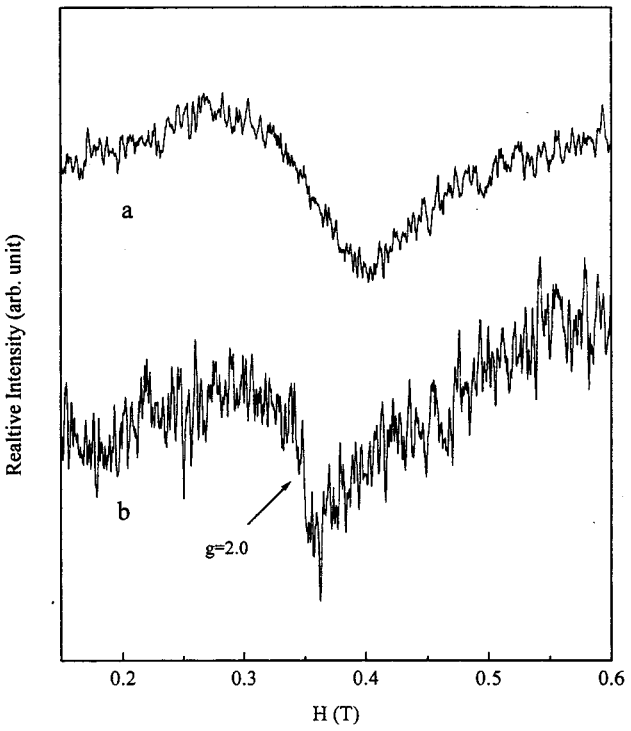

Figure 5. EPR spectra recorded at 80 K for typical solutions $Ce_{0.62}Eu_{0.38}O_{2-\delta}$ (a) and $Ce_{0.83}Tb_{0.17}O_{2-\delta}$ (b).

could not be used for calculating the amount of reduction because of the nonlinear relation between its intensity and the concentration of Ce^{4+} and Ce^{3+} species. We tried to subtract the Ce^{3+} component from our XPS signals in Figure 4a using the standard XPS signals of $Ce^{4+}O_2$ with hydrothermal conditions[10] as the reference. During this process, we assumed that the peak intensity at ca. 916 eV for the present experimental spectra is equal to that for the standard CeO_2 basing on such a fact that the peak at ca. 916 eV is primarily associated with the Ce^{4+} ions. The subtracting results show that the differential spectra exhibit two distinct signals, characteristic for Ce^{3+},[10] at ca. 884.0 and 900.0 eV. A typical subtracting spectrum is shown at the bottom of Figure 4a, clearly indicating the presence of some Ce^{3+} ions in our solid solutions.

EPR spectroscopy is very effective in determining the Ce^{3+} ions in the bulk of our solutions $Ce_{1-x}Eu_xO_{2-\delta}$ because Ce^{4+} and Eu^{3+} are inactive in EPR. The EPR spectrum was recorded at 80 K for a typical solution $Ce_{0.68}Eu_{0.38}O_{2-\delta}$. As shown in Figure 5, within a magnetic field range of 0.15−0.40 T, only one broad signal is observed at $g \sim 2.0$. The presence of this signal suggests that the Ce^{3+} ions only occupied the lattice sites of lower symmetry; otherwise, two distinct EPR signals with $g_\perp \sim 1.97$ and $g_\parallel \sim 1.94$ should be observed due to axis symmetry. Such two signals have been found in CeO_{2-y} and solid solutions $(CeO_2)_{1-x}(BiO_{1.5})_x$.[12,4] It is known that the g tensor for a paramagnetic ion is closely related to the wave function of the electronic ground state and further to the point symmetry of the crystallographic site; i.e., different symmetries of the crystallographic sites often yield different resonance signals.

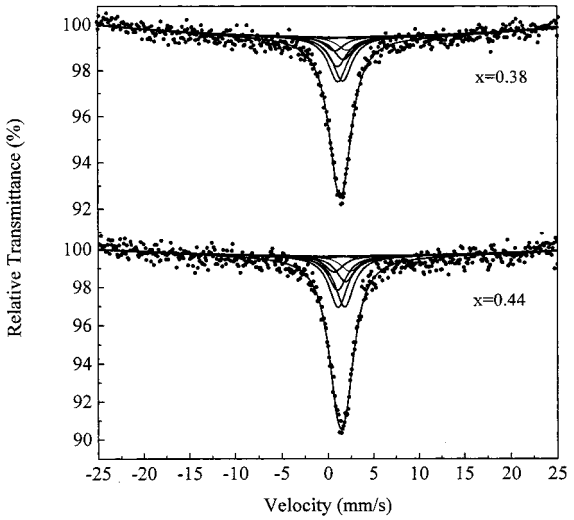

Figure 6. Room temperature ^{151}Eu Mössbauer spectra for the solid solutions $Ce_{1-x}Eu_xO_{2-\delta}$ ($x = 0.38, 0.44$).

It is reasonable that when Ce^{3+} is locating in an asymmetry field, the EPR spectrum will change dramatically. EI-Mallawany et al.[13] reported a broad signal of $g \sim 2.00$ for $(TeO_2)_{0.95}(CeO_2)_{0.05}$, which is very similar to those of our solid solutions. They had ascribed this signal to Ce^{3+}. For our solutions, the broad signal can be associated with Ce^{3+} in an asymmetry field, which is a result of the disordered distribution of oxygen deficiency around the Ce^{3+} ions, i.e., defect associations $\{Eu'_{Ce}V\ddot{o}\}$ and $\{Ce'_{Ce}V\ddot{o}\}$.

The Eu_{4d} core level XPS spectra shown in Figure 4b exhibit two peaks associated with $Eu_{4d_{5/2}}$ and $Eu_{4d_{3/2}}$ core levels, respectively. The binding energy position is at 133.8 eV for $Eu_{4d_{5/2}}$ and 139.5 eV for $Eu_{4d_{3/2}}$. The spin−orbital splitting value for Eu^{3+} ions is 5.7 eV, which is in good agreement with the literature value.[14] No peaks are observed at a lower binding energy. Therefore, Eu ions are present as Eu^{3+} on the sample surfaces of the solid solutions.

The valence states of Eu ions in the bulk of the solutions were determined by ^{151}Eu Mössbauer spectra recorded at room temperature. Figure 6 shows the Mössbauer spectra for the typical solid solutions $Ce_{1-x}Eu_xO_{2-\delta}$ ($x = 0.38, 0.44$). The experimental spectra exhibit only one slightly asymmetric broad single line at ca. 0.0 mm/s, which proves that Eu ions in the solid solutions are in the trivalent state. The half-widths for the absorption lines are very broadened in comparison with that of the natural single line, indicative of the presence of an unresolved quadrupole interaction. The experimental data were all well fitted using 12 transition lines,[15] and the hyperfine parameters are given in Table 1. The isomer shift (IS) of the solid solution $Ce_{0.62}Eu_{0.38}O_{2-\delta}$ (0.07 mm/s) is smaller than that (0.15 mm/s) of $Ce_{0.56}Eu_{0.44}O_{2-\delta}$, which is ascribed to the decrease of the coordination number, i.e., the reduced covalency in the Eu−O bond.[16] The nonzero quadrupole splitting (QS) is ascribed to the local lattice distortion

(12) Abi-aad, E.; Bechara, R.; Grimblot, J.; Aboukais, A. *Chem. Mater.* **1993**, *5*, 793. (b) Oliva, C.; Termignone, G.; Vatti, F. P.; Forni, L.; Vishniakov, A. V. *J. Mater. Sci.* **1996**, *31*, 633.

(13) El-Mallawany, R.; El-Sayed, A. H.; El-Gawad, M. M. H. A. *Mater. Chem. Phys.* **1995**, *41*, 87.

(14) Uwamino, Y.; Ishizuka, T.; Yamatera, H. *J. Electron Spectrosc. Relat. Phenom.* **1984**, *34*, 67.

(15) Su, W.; Liu, X.; Jin, M.; Xu, W.; Wu, D.; Liu, M. *Phys. Rev. B* **1988**, *37*, 35.

Table 1. Hyperfine Parameters for the Typical Solutions $Ce_{1-x}Eu_xO_{2-\delta}$ ($x = 0.38, 0.44$) by High-Temperature and -Pressure Synthesis (vs Eu_2O_3)

sample	IS (mm/s)	QS (mm/s)	η	fwhm (mm/s)
$Ce_{0.62}Eu_{0.38}O_{2-\delta}$	0.07 ± 0.01	-4.2 ± 0.3	0.87 ± 0.05	1.11 ± 0.01
$Ce_{0.56}Eu_{0.44}O_{2-\delta}$	0.15 ± 0.01	-4.9 ± 0.3	0.90 ± 0.05	1.22 ± 0.01

induced by the oxygen deficiencies around Eu ions. The QS value obtained is negative, indicating that the contribution of the lattice to the electric field gradient is larger than that of the 4f electrons.[17]

For the solid solutions $Ce_{1-x}Tb_xO_{2-\delta}$, the XPS measurements give similar Ce_{3d} signals to those in Figure 4a for $Ce_{1-x}Eu_xO_{2-\delta}$. The EPR spectrum was recorded at 80 K for a typical solution $Ce_{0.83}Tb_{0.17}O_{2-\delta}$. As shown in Figure 5b, only one resonance signal was observed at ca. $g \sim 2.0$, which is similar to that of the solid solutions $Ce_{1-x}Eu_xO_{2-\delta}$ in Figure 5a. Therefore, Ce^{3+} ions are also present in the bulk of the solid solutions $Ce_{1-x}Tb_xO_{2-\delta}$. Tb_{4d} core level XPS spectra for the solid solutions $Ce_{1-x}Tb_xO_{2-\delta}$ are shown in Figure 7. For comparison, we also illustrate the Tb_{4d} spectra for some typical oxides containing pure Tb^{3+} and Tb^{4+} ions. The difference between $Tb^{3+}{}_{4d}$ and $Tb^{4+}{}_{4d}$ spectra is clearly seen. For the pure Tb^{3+} ion, the main photoelectron line position for Tb_{4d} is at ca. 150.0 eV, and no other photoelectron lines are observed at ca. 157.0 eV. For the pure Tb^{4+} ions, however, two strong photoelectron lines are at ca. 157.0 and 150.0 eV, respectively. Therefore, the photoelectron line at ca. 157.0 eV can be used to identify Tb^{4+} ions in the solutions. The Tb_{4d} spectra for our solid solutions $Ce_{1-x}Tb_xO_{2-\delta}$ synthesized by high-temperature and -pressure are nearly the same as those for $Tb^{3+}FeO_3$. This fact suggests that all Tb ions are present as Tb^{3+} in our solid solutions. It should be noted that the starting material used for synthesizing the present solid solutions is Tb_4O_7, in which the Tb ions are present as a mixed valence of Tb^{3+}/Tb^{4+}. During the high-temperature and -pressure synthesis process, all Tb^{4+} ions are reduced into Tb^{3+}. This is different from that of the counterpart by hydrothermal conditions[5] where Tb^{4+} ions had been identified by X-ray absorption near edge spectroscopy.

3. Structural Stability of the Solid Solutions $Ce_{1-x}RE_xO_{2-\delta}$ (RE = Eu, Tb). As described in the Experimental Section for impedance measurements, the pellet samples had been heated at 550 °C to remove completely the organic components in the silver paste. It appears necessary here to examine the structural stabilities of the as-prepared solid solutions $Ce_{1-x}RE_xO_{2-\delta}$ (RE = Eu, Tb) up to 550 °C. We annealed the solid solutions at 550 °C in air for 2 h and measured the XRD patterns of the annealed products. The XRD pattern for the annealed product of a typical solid solution $Ce_{0.80}Eu_{0.20}O_{2-\delta}$ is shown in Figure 8a. It is clear that the structure of the annealed product is nearly the same as that before annealing, shown in Figure 1. Other compositional solutions $Ce_{1-x}Eu_xO_{2-\delta}$ give similar results. This fact indicates that solid solutions $Ce_{1-x}Eu_xO_{2-\delta}$ are stable up to 550 °C.

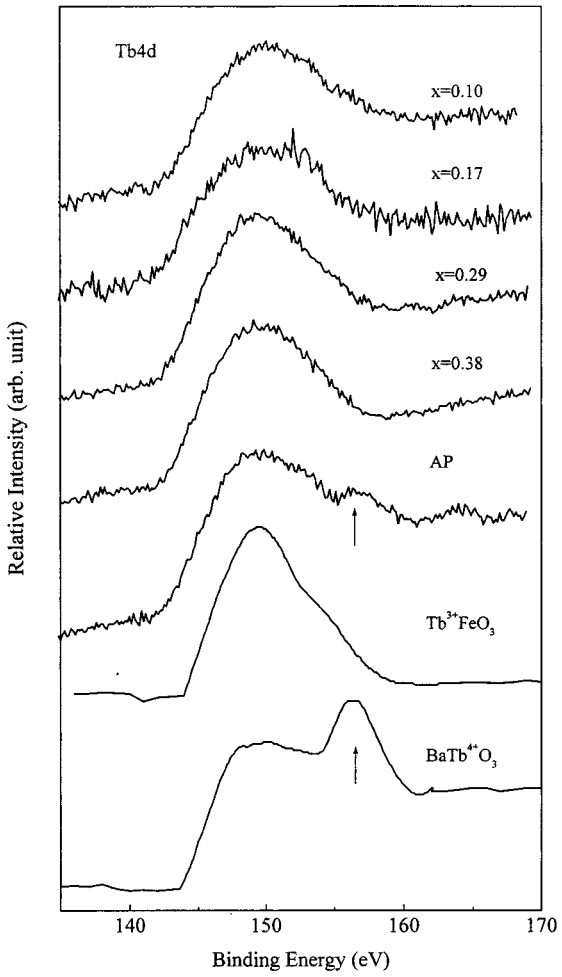

Figure 7. Core level XPS of Tb_{4d} for the solid solutions $Ce_{1-x}Tb_xO_{2-\delta}$ ($x = 0.10, 0.17, 0.29, 0.38$) and AP (the product by annealing the solution $Ce_{0.71}Tb_{0.29}O_{2-\delta}$ at 550 °C in air for 2 h). XPS spectra for the standard samples $Tb^{3+}FeO_3$ and $BaTb^{4+}O_3$ were also shown for comparison. The photoelectron peaks marked by arrows are characteristic for Tb^{4+} ions.

However, the solid solutions $Ce_{1-x}Tb_xO_{2-\delta}$ synthesized by high-temperature and -pressure are metastable. XRD patterns for the solutions $Ce_{1-x}Tb_xO_{2-\delta}$ ($x = 0.29, 0.38$) change obviously after annealing. All diffraction peaks in Figures 8b and 8c for the samples after annealing are split into two peaks. XRD data analysis shows that the decomposition products after annealing are mixtures of two fluorite phases, suggesting a phase separation process. To investigate the mechanism for the phase separation process, we measured the Tb_{4d} core level XPS of the annealed product (AP) of a typical solution $Ce_{0.71}Tb_{0.29}O_{2-\delta}$. The XPS spectra for the standard samples $Tb^{3+}FeO_3$ and $BaTb^{4+}O_3$ were also shown for comparison. As shown in Figure 7, a weak photoelectron peak is observed at ca. 157.0 eV, clearly showing that Tb^{3+} ions are partially oxidized into Tb^{4+} during the annealing process. Theoretically, complete oxidation of Tb^{3+} to Tb^{4+} in $Ce_{0.71}Tb_{0.29}O_{2-\delta}$ (here, all Ce ions were assumed to be Ce^{4+}) will bring about a total weight gain of ca. 1.3%. Our TG measurement shown in Figure 9 gives a weight gain of 0.4% at ca. 350 °C, which also proves the oxidation process of ca. 30% Tb^{3+} to Tb^{4+}. One should admit that there exists an obvious difference between the dynamic heating of TG measurements and

(16) Tanabe, S.; Hirao, K.; Soga, N. *J. Non-Cryst. Solids* **1989**, *113*, 178.

(17) Chien, C. L.; Sleight, A. W. *Phys. Rev. B* **1978**, *18*, 2031.

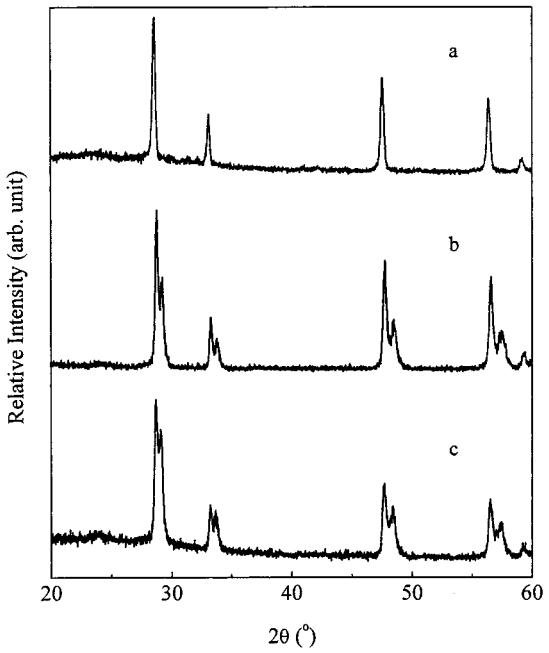

Figure 8. XRD patterns for the product obtained by annealing the solid solutions $Ce_{0.80}Eu_{0.20}O_{2-\delta}$ (a), $Ce_{0.71}Tb_{0.29}O_{2-\delta}$ (b), and $Ce_{0.62}Tb_{0.38}O_{2-\delta}$ (c) at 550 °C in air for 2 h.

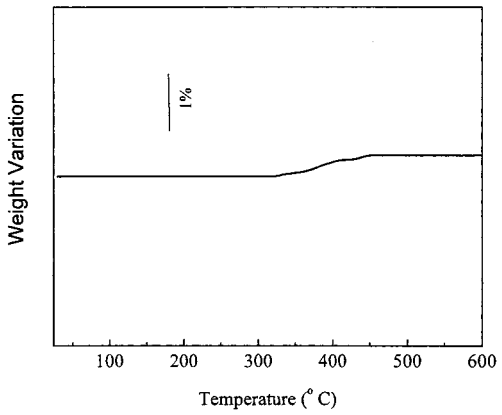

Figure 9. TG curve for the typical solution $Ce_{0.71}Tb_{0.29}O_{2-\delta}$ measured in air.

the annealing conditions, but both experiments confirm such a conclusion: the solid solution $Ce_{0.71}Tb_{0.29}O_{2-\delta}$ is metastable and the decomposition is accompanied with an oxidation process at a higher temperature up to 550 °C. Similar decomposition and oxidation processes have been found in other compositional solid solutions $Ce_{1-x}Tb_xO_{2-\delta}$. In combination with the results of Greenblatt et al.,[5] e.g., mixed valence feature of Tb^{3+}/Tb^{4+} and the corresponding higher thermal stability of the fluorite structure, it can be concluded that the metastable fluorite structures of the solid solutions $Ce_{1-x}Tb_xO_{2-\delta}$ by present high-temperature and -pressure synthesis are closely related to the pure Tb^{3+} occupation in the fluorite lattice.

4. Transport Properties for the Solid Solutions $Ce_{1-x}RE_xO_{2-\delta}$ (RE = Eu, Tb). The conductivities for the solid solutions $Ce_{1-x}RE_xO_{2-\delta}$ (RE = Eu, Tb) are measured by the ac complex impedance technique. All impedance plots show primarily one distinct depressed semicircle at higher frequencies, which is attributed to the bulk effect, while the arc at lower frequencies

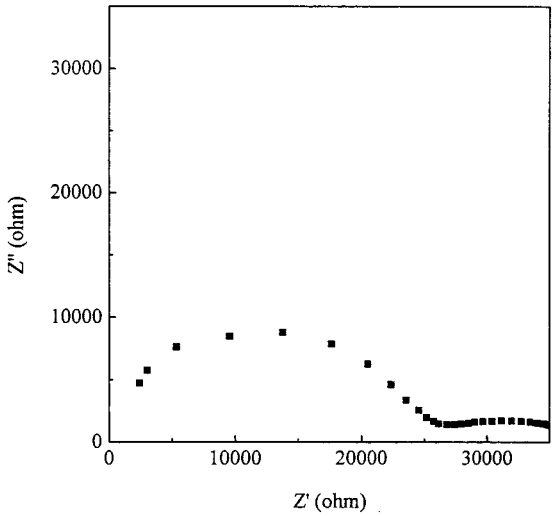

Figure 10. Typical impedance spectrum for the solution $Ce_{0.80}Eu_{0.20}O_{2-\delta}$ at 550 °C.

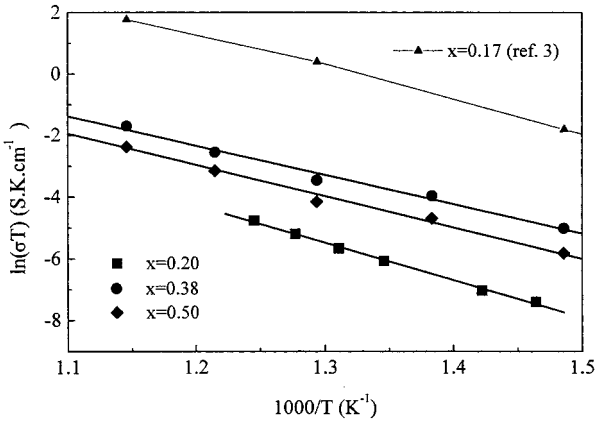

Figure 11. Temperature dependence of the conductivity for the solid solutions $Ce_{1-x}Eu_xO_{2-\delta}$ (x = 0.20, 0.38, 0.50). The conductivity data for the best conducting phase x = 0.17 by the hydrothermal conditions (ref 3) are also shown for comparison.

associated with the grain boundary conduction is not obvious. Figure 10 illustrates a typical impedance plot for the solid solution $Ce_{0.80}Eu_{0.20}O_{2-\delta}$ measured at 550 °C. The relaxation phenomena or oxygen exchange processes ascribable to the interface between the electrodes and the samples are not observed because of no spike existing in the lower frequency range. Chiodelli et al.[18] studied systematically the electrical properties of some ceria-based solid solutions and they found that the absence of the electrode arc contribution was due to the partial electronic nature of the conductivity in the ceria-based solid solutions. The electronic component of the conductivity for the present solid solutions $Ce_{1-x}Eu_xO_{2-\delta}$ should be closely related to the presence of Ce^{3+} due to the existence of reduction equilibrium (Ce^{4+}/Ce^{3+}). The conductivity is determined by the intersection of the corresponding semicircles on the real part of the impedance axis. Figure 11 gives ln σT versus $1/T$ plots for the solid solutions $Ce_{1-x}Eu_xO_{2-\delta}$ (x = 0.20, 0.38, 0.5). It is clear that the conductivity data for these solutions show only one linear region. The conductivity–

(18) Chiodelli, G.; Flor, G.; Scagliotti, M. *Solid State Ionics* **1996**, *91*, 109 and references therein.

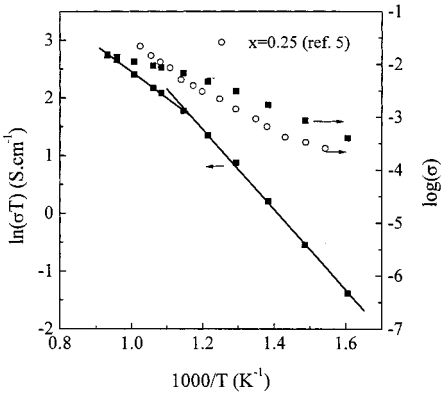

Figure 12. Temperature dependence of the conductivity for the decomposition product of a typical solution $Ce_{0.71}Tb_{0.29}O_{2-\delta}$. The conductivity data (log σ) for the solid solution $Ce_{0.75}Tb_{0.25}O_{2-\delta}$ by the hydrothermal conditions (ref 5) along with our data are also shown for comparison (right axis). It is clear that both samples have comparable ionic conductivity.

temperature dependencies exhibit Arrhenius behavior over the temperature regions studied, showing primarily oxide ion conduction. The activation energies (E_a) obtained by the slope of the experimental data are 1.05, 0.82, and 0.87 eV for the solutions with $x = 0.20$, 0.38, and 0.5, while the corresponding conductivities measured at 550 °C are 1.69×10^{-5}, 9.58×10^{-5}, and 5.22×10^{-5} S/cm, respectively, which were comparable with those reported by Kodo et al.[19] The variation trends of E_a (first decrease and then increase) and the corresponding conductivity (just opposite to E_a) reflect the same mechanism as that mentioned above for the nonlinear relationship between the lattice parameter and dopant content. Similar trends had been found in the $Ce_{1-x}Sm_xO_{2-x/2}$ and $Ce_{1-x}Ca_xO_{2-x}$ solid solutions[3] (as described in the Introduction). However, the conductivity data shown in Figure 12 for the decomposition product of the solution $Ce_{0.79}Tb_{0.21}O_{2-\delta}$ give two linear regions. The activation energy is 0.60 eV within 350−600 °C, whereas above 600 °C, the activation energy is reduced to 0.39 eV. At 720 °C, the conductivity reaches as high as 1.1×10^{-2} S/cm, comparable with the maximum of the total conductivity ($\sigma_{700°C} = 2.1 \times 10^{-2}$ S/cm) for the solution $Ce_{0.75}Tb_{0.25}O_{2-x}$ by hydrothermal conditions.[5] This higher conductivity is believed to be closely related to an electronic component involved due to the presence of two types of mixed valences, Tb^{3+}/Tb^{4+} and Ce^{3+}/Ce^{4+} in the decomposition product of the solution $Ce_{0.71}Tb_{0.29}O_{2-\delta}$, as revealed by TG, XPS, and impedance plots.

(19) Kudo, T.; Obayashi, H. *J. Electrochem. Soc.* **1975**, *122*, 142.

Conclusions

This work reports on the stabilization of Eu^{3+} and Tb^{3+} ions in the ceria lattice by high-temperature and -pressure synthesis of the single-phase fluorite solutions $Ce_{1-x}RE_xO_{2-\delta}$ (RE = Eu, Tb). Both series of solid solutions containing pure trivalent dopants have nonlinear relationships between the lattice parameter and dopant content. The solid solutions $Ce_{1-x}Eu_xO_{2-\delta}$ are thermally stable up to 550 °C, while the solutions $Ce_{1-x}Eu_xO_{2-\delta}$ have metastable fluorite structures and will be decomposed into two fluorite phases at temperatures <550 °C, accompanied by partial oxidation from Tb^{3+} to Tb^{4+}. The conductivity data for the solid solutions $Ce_{1-x}Eu_xO_{2-\delta}$ showed one linear region, whereas for the decomposition product of the solution $Ce_{0.71}Tb_{0.29}O_{2-\delta}$, the conductivity data gave two linear regions. The variation trends for the lattice parameter and conductivity data were ascribed to the results of cation substitution and the variations of the relative contents of oxygen vacancy and defect associations. At 720 °C, the conductivity for the decomposition product of the solution $Ce_{0.71}Tb_{0.29}O_{2-\delta}$ reached as high as 1.1×10^{-2} S/cm, which was explained in terms of an electronic component involved due to the presence of mixed valences, Tb^{3+}/Tb^{4+} and Ce^{3+}/Ce^{4+}.

Acknowledgment. This project was financially supported by funding from NSFC (19804005) (L.L.).

CM990803P